

## Supporting Information

### **Ni<sub>3</sub>S<sub>2</sub> Anchored into N/S co-doped Reduced Graphene Oxide with Highly Pleated Structure as a Sulfur Host for Lithium-Sulfur Batteries**

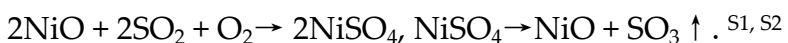
**Daying Guo,<sup>a</sup> Zihe Zhang,<sup>c</sup> Bin Xi,<sup>a,\*</sup> Zhisheng Yu,<sup>b</sup> Zhen Zhou<sup>c,\*</sup> and Xi'an Chen<sup>b,\*</sup>**

<sup>a</sup> School of Materials Science and Engineering, Sun Yat-sen University, Guangzhou, China 510275; <sup>b</sup> Key Laboratory of Carbon Materials of Zhejiang Province, College of Chemistry and Materials Engineering, Wenzhou University, Wenzhou, China 325035; <sup>c</sup> Tianjin Key Laboratory of Metal and Molecule Based Material Chemistry Key Laboratory of Advanced Energy Materials Chemistry (Ministry of Education); Institute of New Energy Material Chemistry Collaborative Innovation Center of Chemical Science and Engineering (Tianjin); School of Materials Science and Engineering National Institute for Advanced Materials Nankai University Tianjin, China 300350

\* To whom correspondence should be addressed. E-mail: [xibin3@mail.sysu.edu.cn](mailto:xibin3@mail.sysu.edu.cn); [zhouzhen@nankai.edu.cn](mailto:zhouzhen@nankai.edu.cn); [xianchen@wzu.edu.cn](mailto:xianchen@wzu.edu.cn)

### **Materials Characterization**

The weight percentages of Ni<sub>3</sub>S<sub>2</sub> in the composites were measured using a TG/DTA thermo-gravimetric analyzer (Diamond PE) under an O<sub>2</sub> atmosphere at a heating rate of 10 °C min<sup>-1</sup> from room temperature to 950 °C, with a flow rate of 80 mL min<sup>-1</sup>. The oxidation of Ni<sub>3</sub>S<sub>2</sub> in O<sub>2</sub> goes through multiple steps:



## Electrochemical measurements

Galvanostatic charge/discharge tests were conducted on fabricated CR2025-type coin battery, to evaluate the electrochemical capacity and cycle stability of the electrodes on the basis of the active sulfur at current densities of 0.2 C, 0.5 C, 1 C, 2 C, 3 C, 5 C (1 C = 1675 mA h g<sup>-1</sup>) from 1.5 to 3.0 V using a LANHE instrument. Cyclic Voltammetry data were recorded on a CHI660e electrochemical workstation between 1.8 and 2.6 V to characterize the redox behavior and the kinetic reversibility of the cell. The AC impedance was measured with fresh cells at the open circuit potential. This was also carried out using a CHI 760e electrochemical workstation. The ac amplitude was 5 mV and the frequency ranged from 100 kHz to 0.01 Hz. In addition, the amount of electrolyte is maintained to ~15  $\mu\text{L}/\text{mg}$  (sulfur) for the batteries cathode with the low sulfur areal density, ~12  $\mu\text{L}/\text{mg}$  (sulfur) for the batteries cathode with the high sulfur areal density.

**Elevate loading of sulfur.** High sulfur loading on the cathode is helpful to obtain high energy density batteries. Therefore, the effects of different sulfur loading on the performance of batteries are studied (**Figure S22**). When the percentages of sulfur loaded are 61% and 81% (**Figure S22a**), the reversible discharge capacity are 1664.5 mAh g<sup>-1</sup> and 1346.8 mAh g<sup>-1</sup> at 0.2 C (**Figure S22b**), respectively, corresponding to active material utilization rate of 99.4% and 80.4%. It can be seen that as the sulfur loading increases, the specific discharge capacity decreases gradually. The capacity obtained at various rates are shown in **Table S9**. Interestingly, even 81% sulfur was loaded, corresponding discharge capacity still reaches 1346.8 mAh g<sup>-1</sup> at 0.2 C and 762.9 mAh g<sup>-1</sup> at 25-fold current density, i.e. 5 C (**Figure S22b**). As shown in **Figure S22c**, the discharge capacity of 3/S 81% is 972.6 mAh g<sup>-1</sup> in the 1<sup>st</sup> cycle at 1 C and the decay rate is 0.11% per cycle after 500 cycles. Regarding to 3/S 61%, the results that initial capacity of 1258.6 mA h g<sup>-1</sup> dropped to 778.3 mA h g<sup>-1</sup> over 500 charge-discharge cycle at 1 C and the decay rate of

0.076% per cycle, represent the fastest capacity retention and most stable performance.

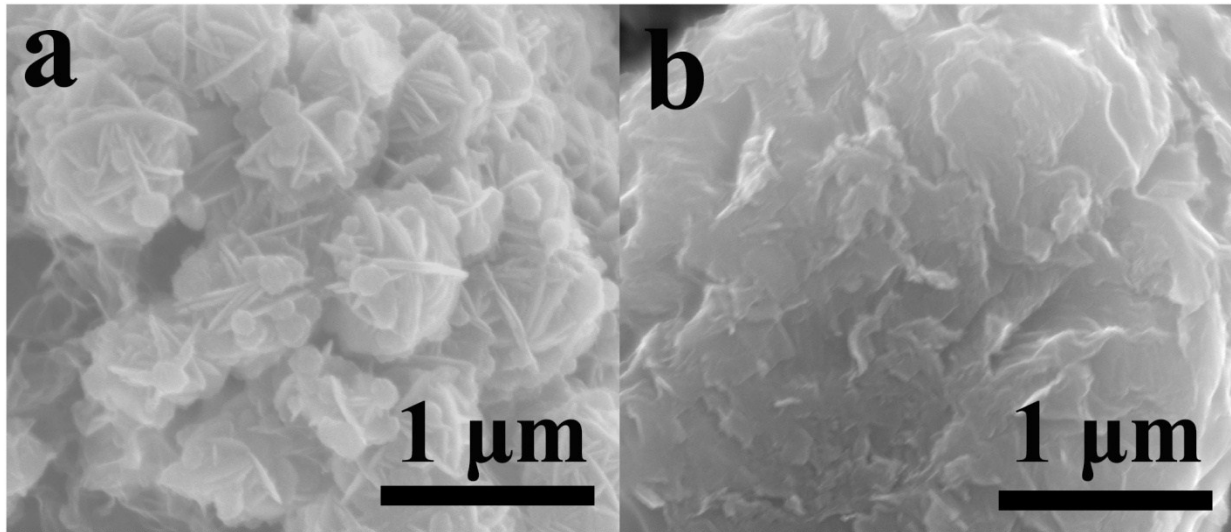


**Figure S1.** SEM images of Ni<sub>3</sub>S<sub>2</sub>-800°C (a), composite 1 (b)

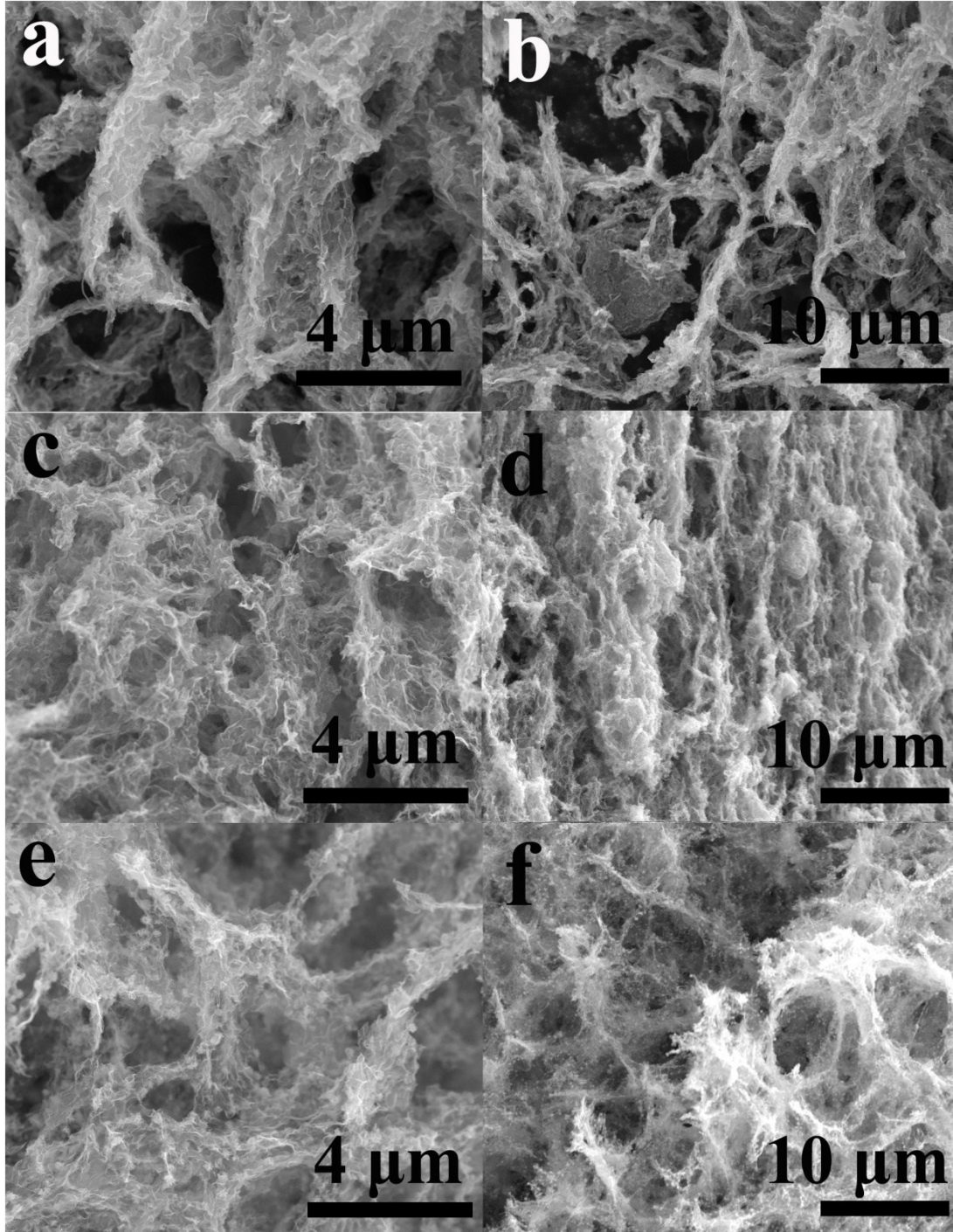


**Figure S2.** SEM images of composites 2 (a, b), 3 (c, d) and 4 (e, f)

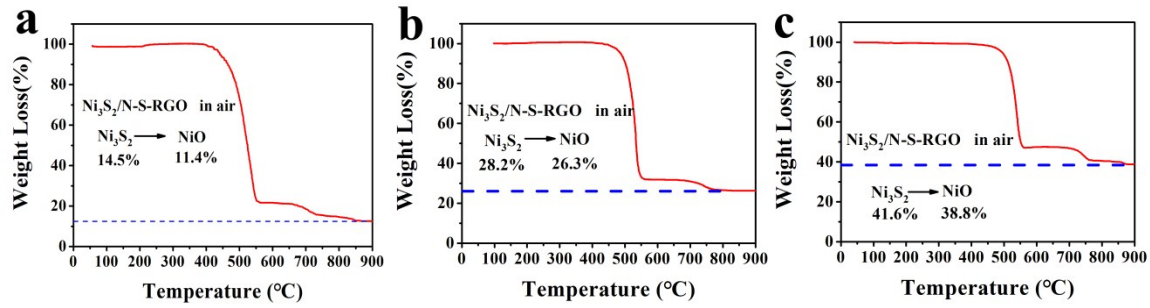


Figure S3. TGA images of 2 (a), 3 (b) and 4 (c)

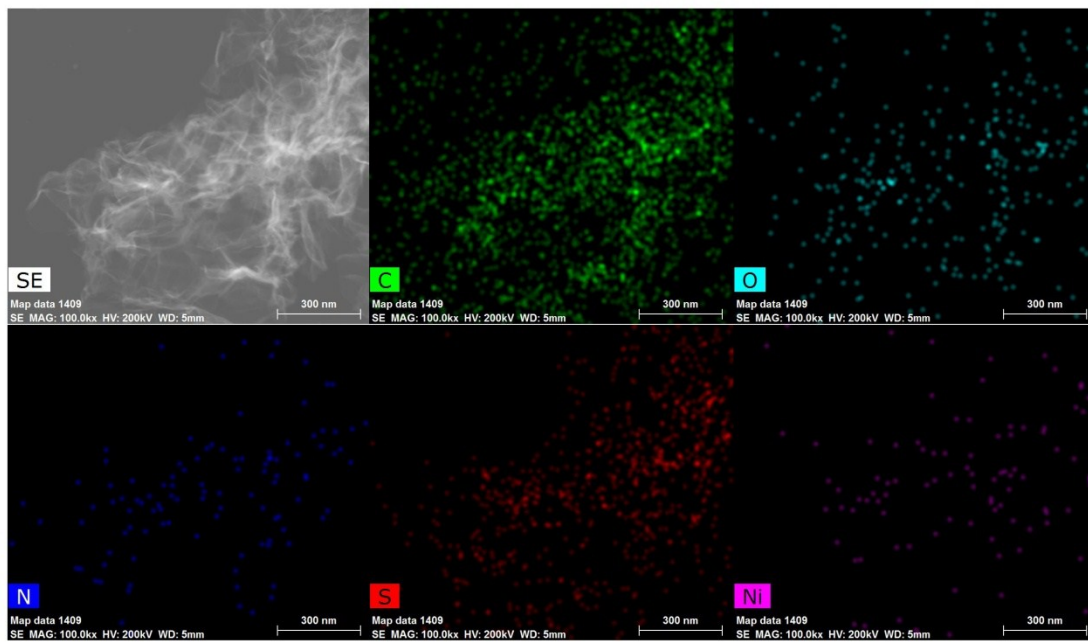


Figure S4. TEM image and EDS elemental mapping of composite 3.

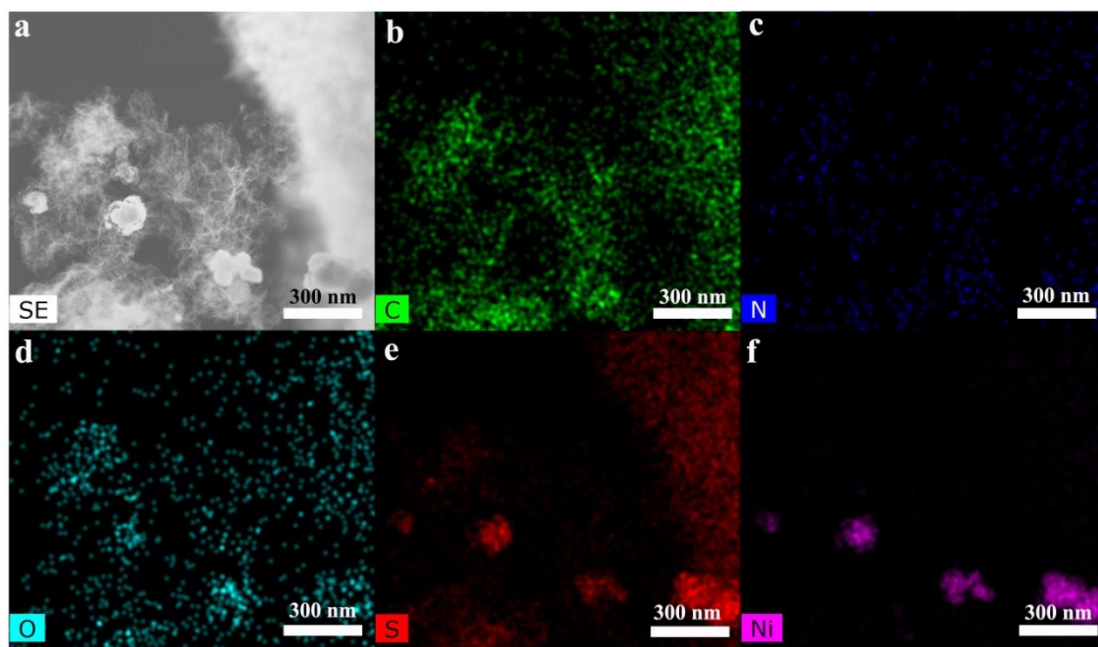


Figure S5. TEM image and EDS elemental mapping of composite 4.

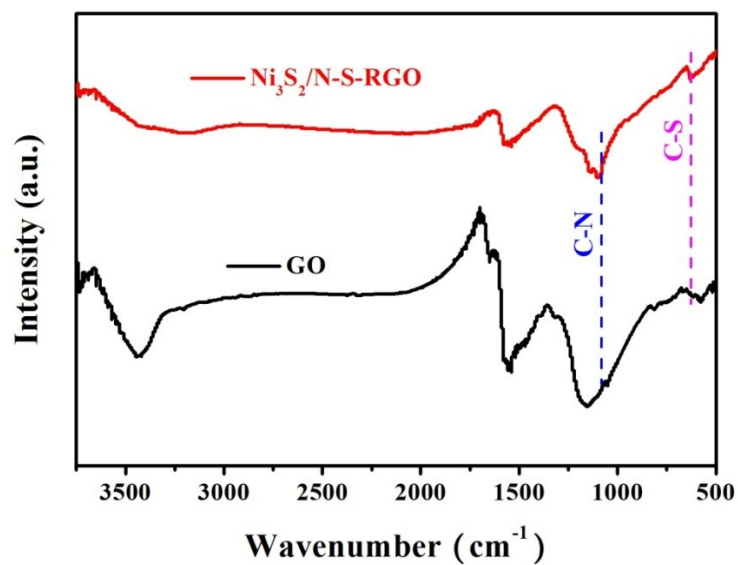
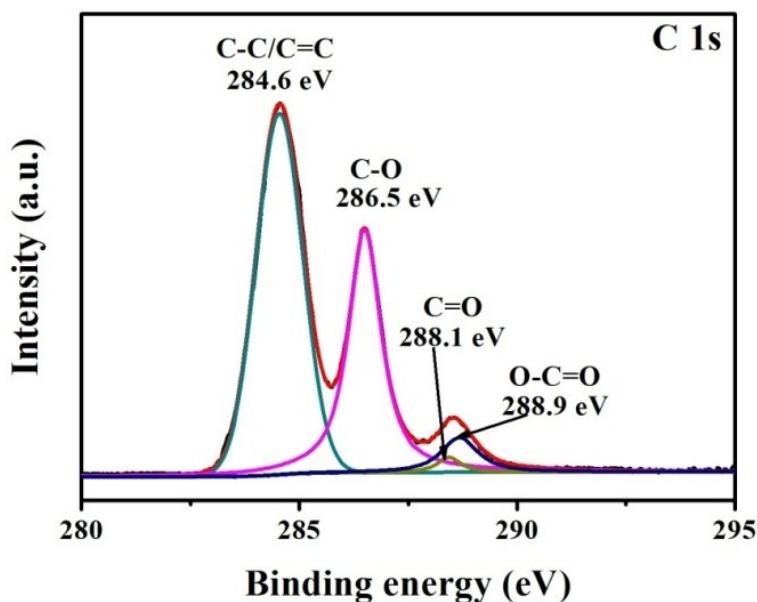
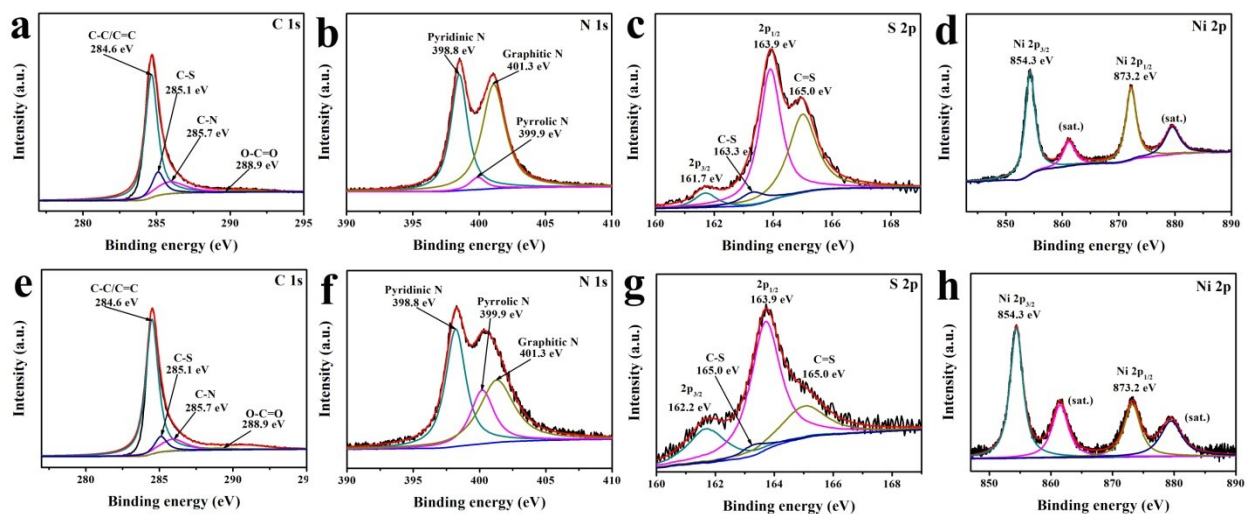


Figure S6. FTIR spectra of GO and  $\text{Ni}_3\text{S}_2/(\text{N}, \text{S})\text{-RGO}$ .



**Figure S7.** High resolution XPS of C 1s in GO.



**Figure S8.** High resolution XPS of (a) C 1s, (b) N 1s, (c) S 2p and (d) Ni 2p in composite **2**. (e) C 1s, (f) N 1s, (g) S 2p and (h) Ni 2p of composite **4**.

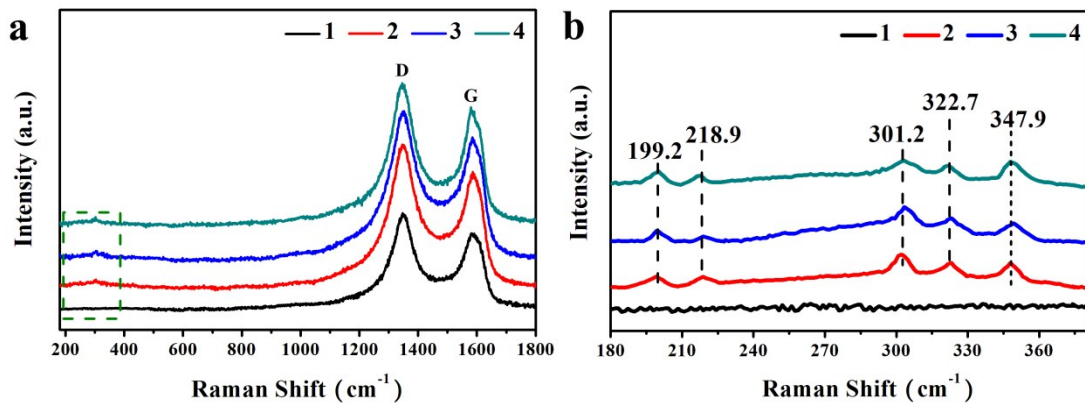


**Figure S9.** (a) Raman spectra of composites 1, 2, 3 and 4; (b) the enlarged part of the green marked area in (a);

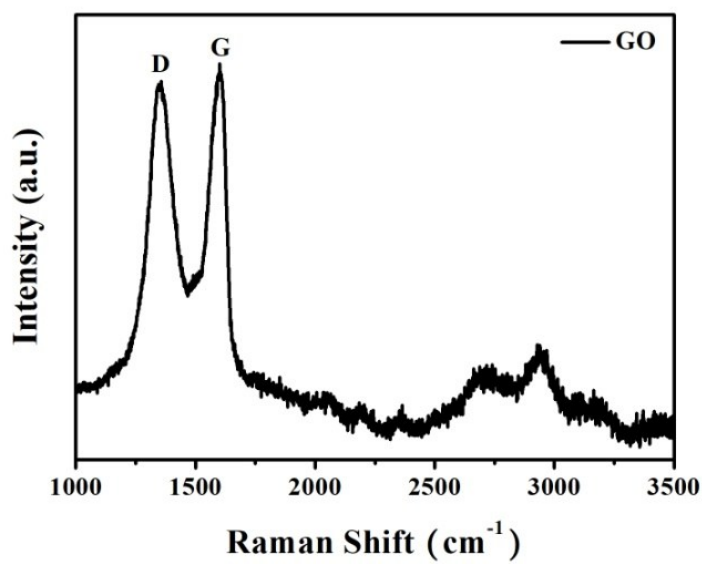


**Figure S10.** Raman spectra of GO

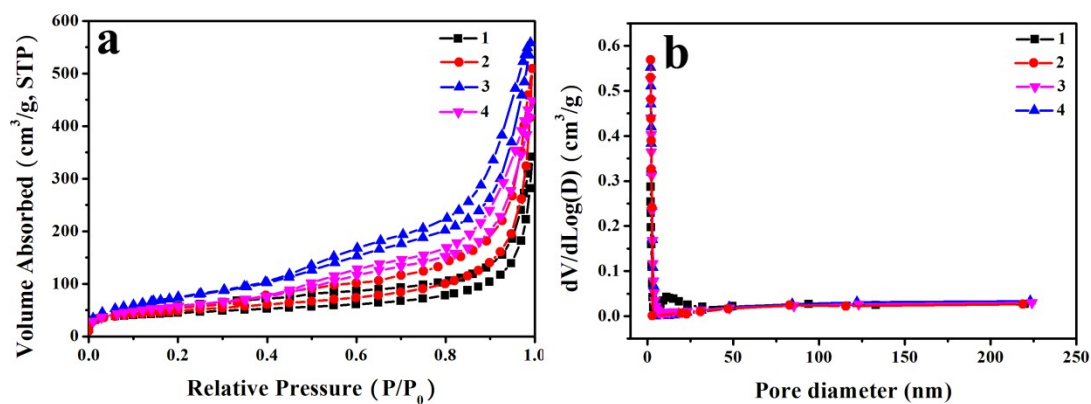


**Figure S11.** (a) N<sub>2</sub> adsorption/desorption isotherm (b) the curves for the corresponding pore size distribution of composites 1, 2, 3 and 4.

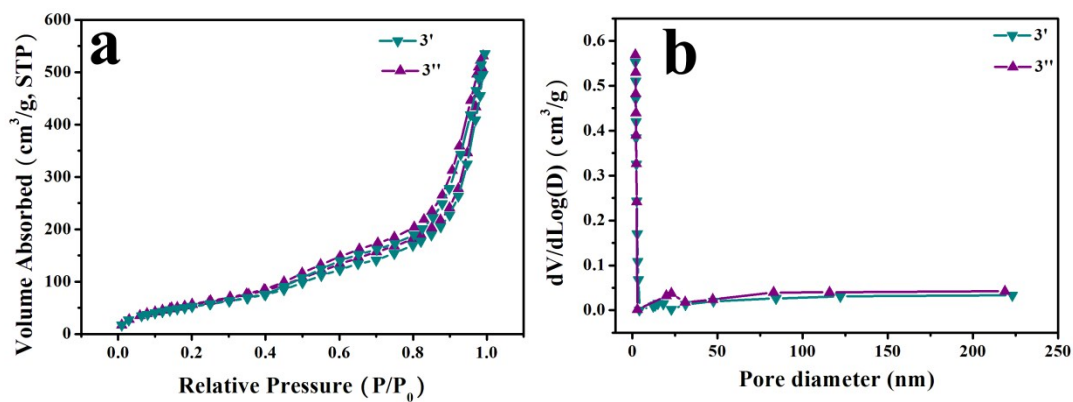


**Figure S12.** (a) N<sub>2</sub> adsorption/desorption isotherm (b) the curves for the corresponding pore size distribution of composites 3', and 3''.

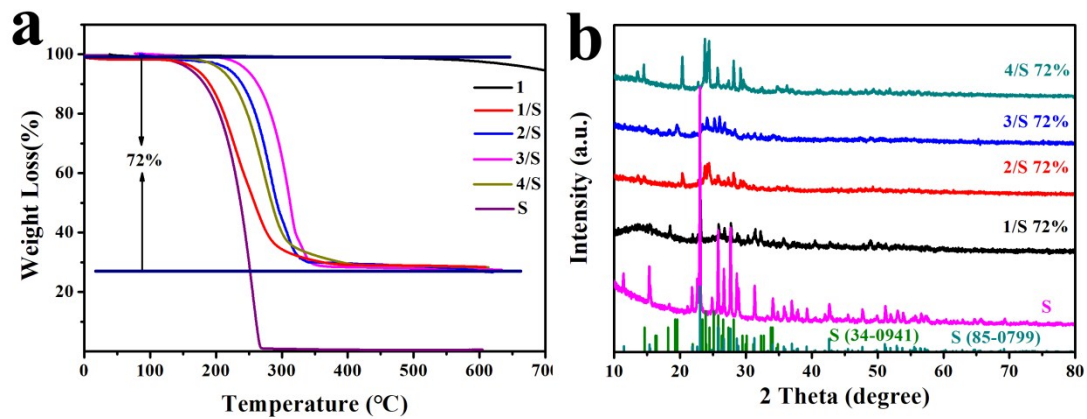


Figure S13. (a) TGA curves and (b) XRD patterns of S, composites 1, 2, 3 and 4.

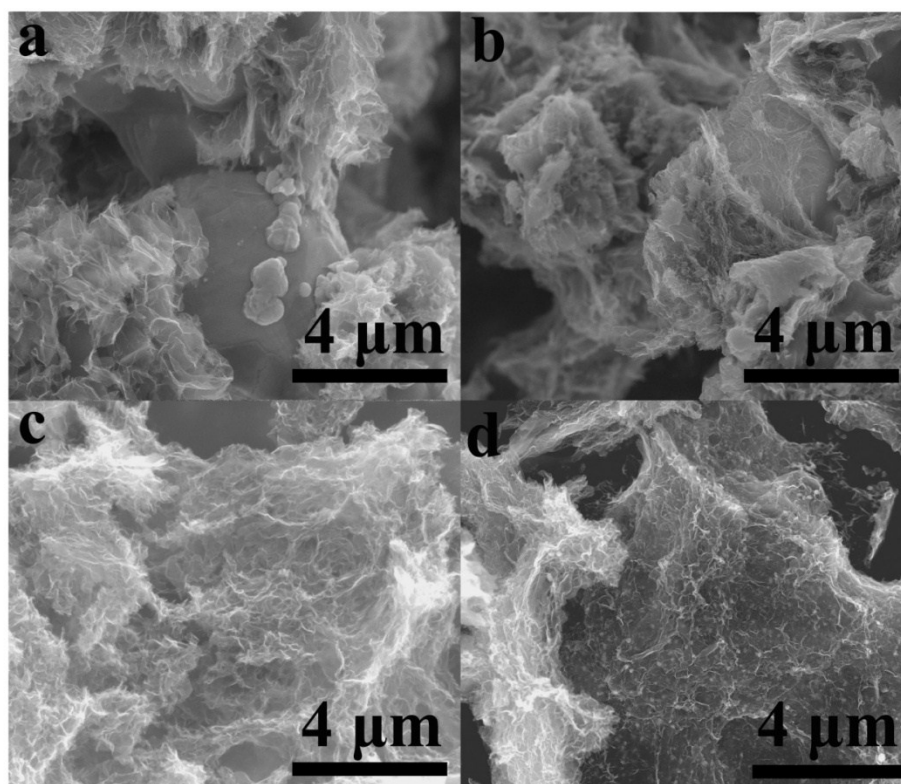
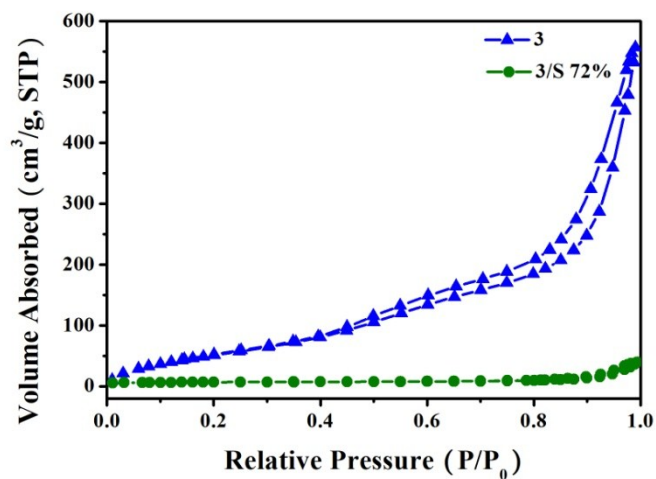
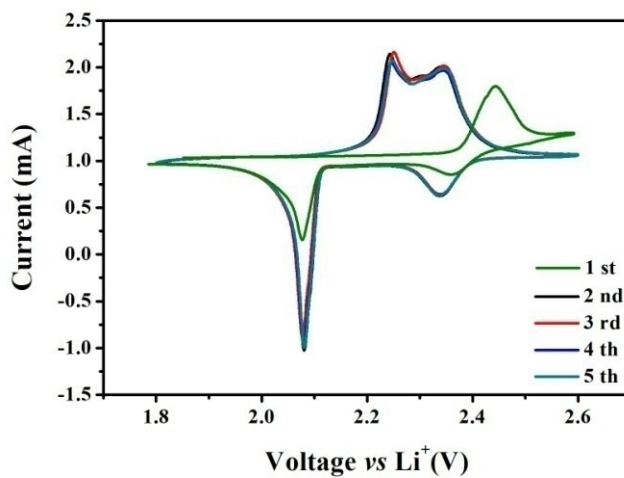


Figure S14. SEM images of (a) 1/S 72%, (b) 2/S 72%, (c) 3/S 72% and (d) 4/S 72%.



**Figure S15.** N<sub>2</sub> adsorption/desorption isotherm of composites **3** and **3/S 72%**.



**Figure S16.** Typical CV curve of the **3/S 72%/Li** cell at a scan rate of 0.1 mV s<sup>-1</sup>.

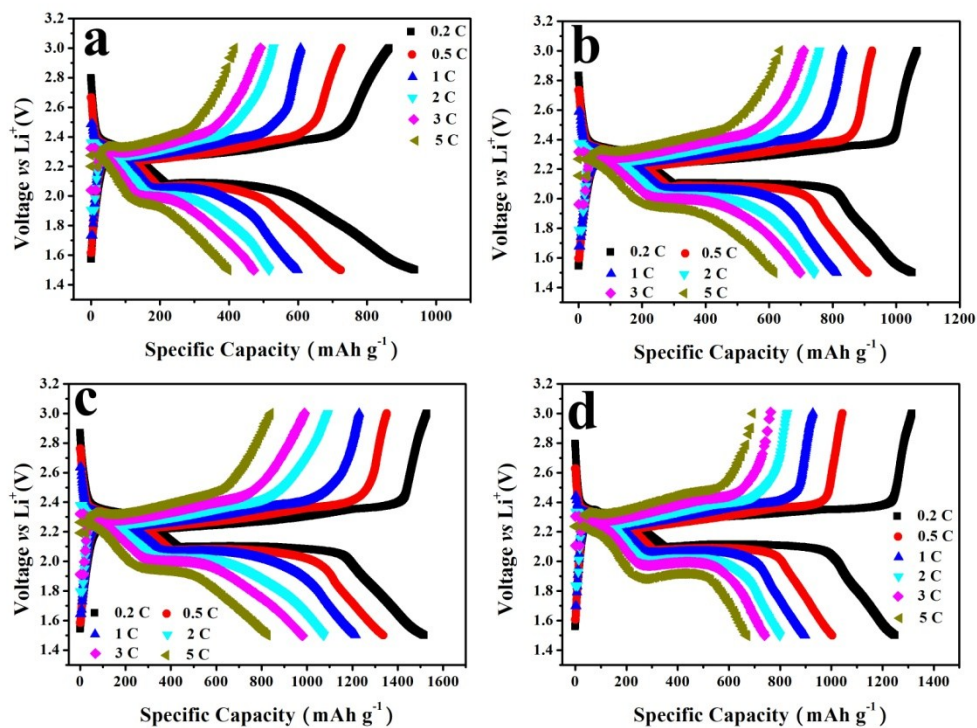


**Figure S17.** Discharge-charge curves recorded at different rates for composites (a) 1/S 72%, (b) 2/S 72%, (c) 3/S 72% and (d) 4/S 72%/Li cells.

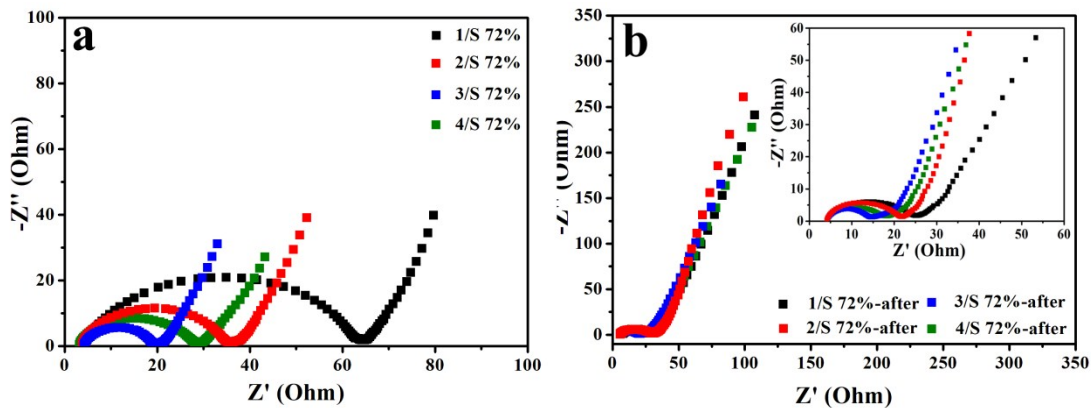


**Figure S18.** The Nyquist plots of (a) before and (b) after 500 cycles of battery testing on composites 1/S 72%, 2/S 72%, 3/S 72% and 4/S 72%/Li cells.

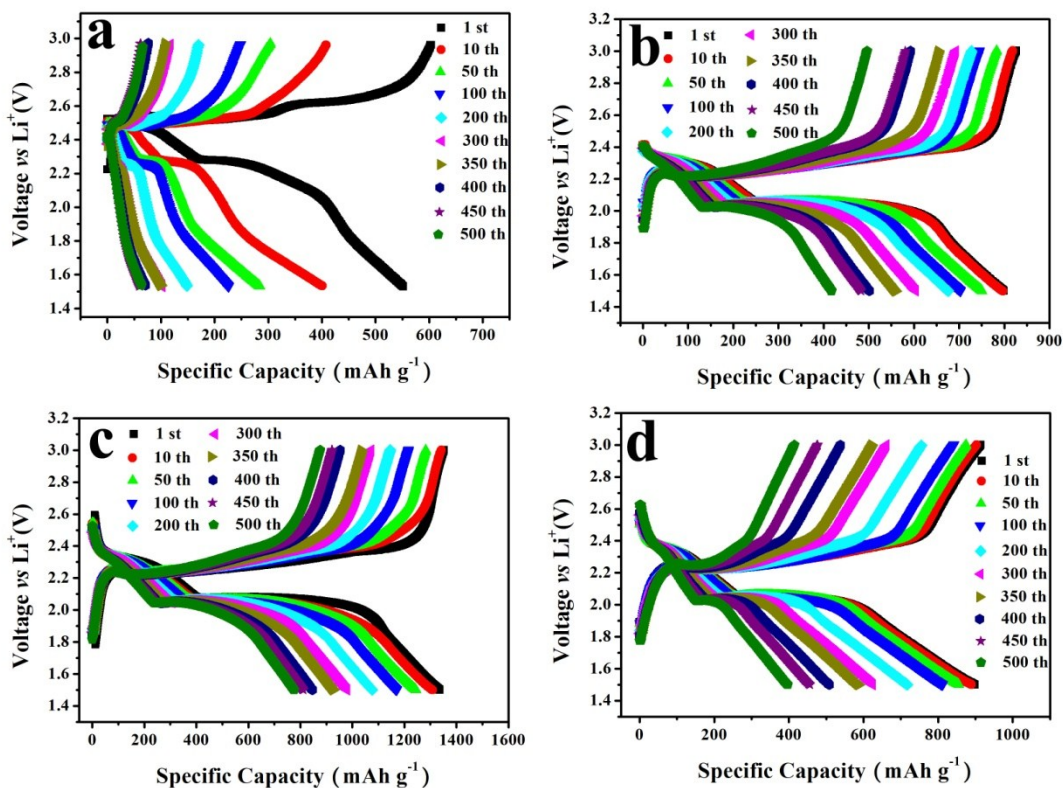


**Figure S19.** Galvanostatic discharge-charge curves recorded at different cycles for composites (a) 1/S 72%, (b) 2/S 72%, (c) 3/S 72% and (d) 4/S 72%/Li cells.

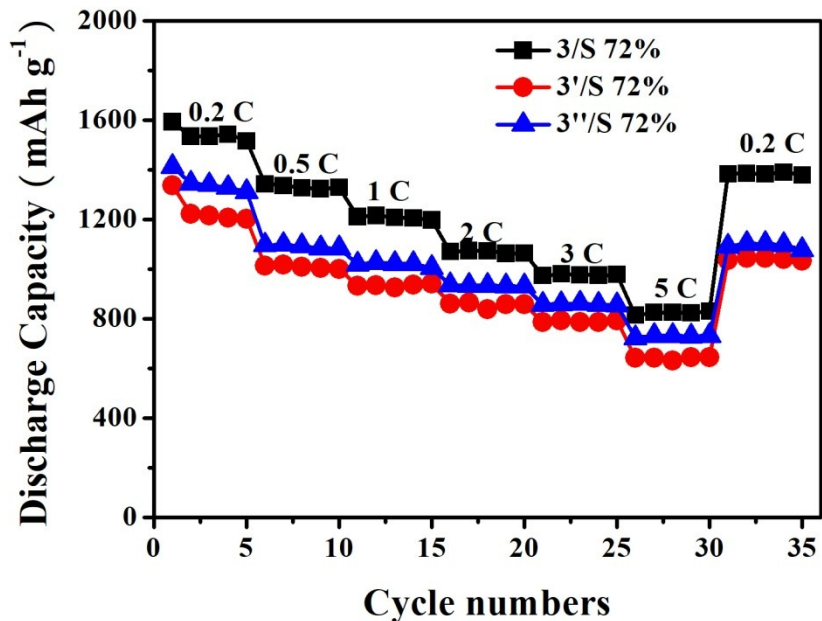


**Figure S20.** Reversible capacity *vs.* current density (rate capability) of the cells with the as-prepared 3/S 72%, 3'/S 72% and 3''/S 72% cathodes.

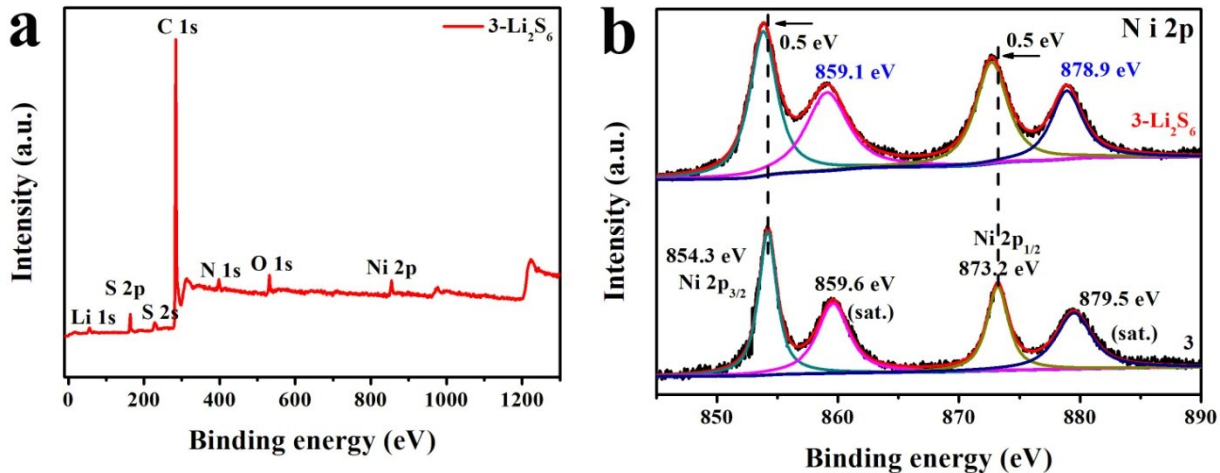


**Figure S21.** XPS survey spectrum of sample  $\text{Li}_2\text{S}_6$ -treated composite **3** ( $3\text{-Li}_2\text{S}_6$ ); (e) XPS spectra of Ni 2p regions for the **3** and  $3\text{-Li}_2\text{S}_6$ .

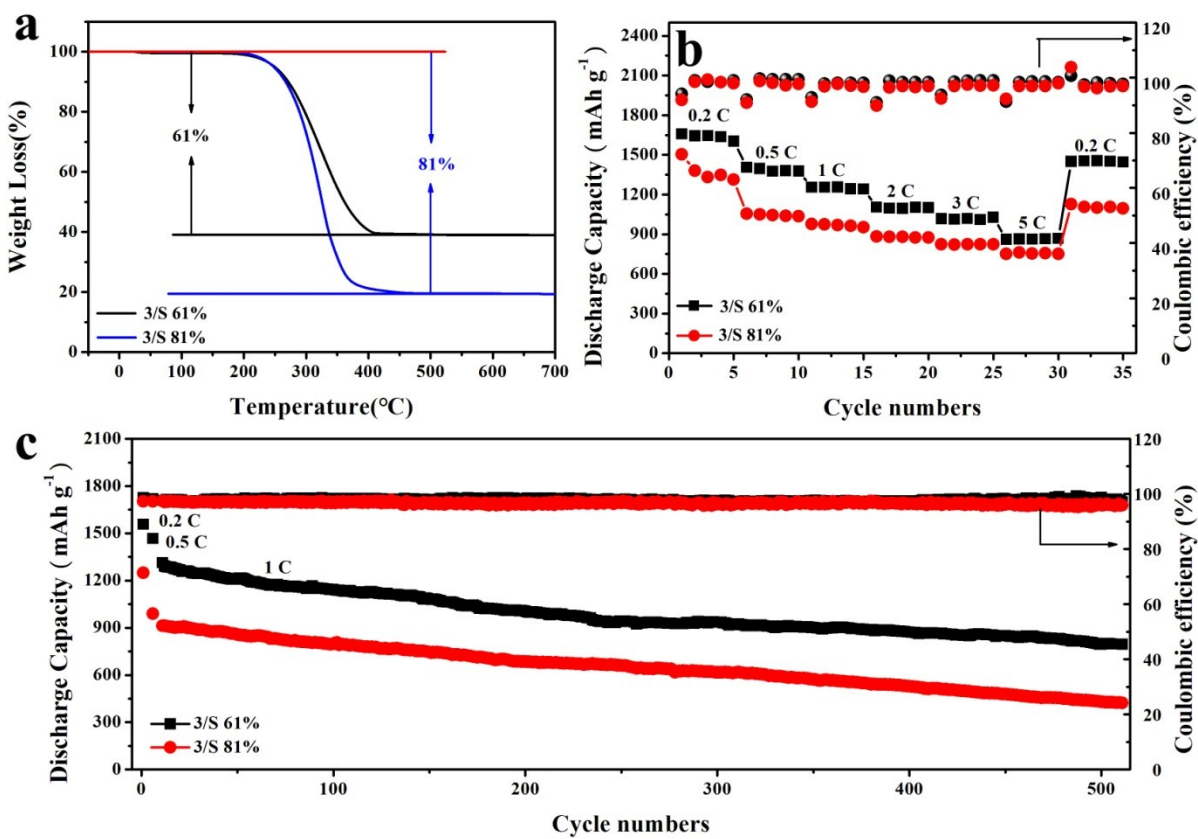


**Figure S22.** (a) TGA curves; (b) rate capability; (c) cycle performance at constant current rate of 1 C and corresponding Coulombic efficiency of the cells with 3/S 61% and 3/S 81% cathodes.

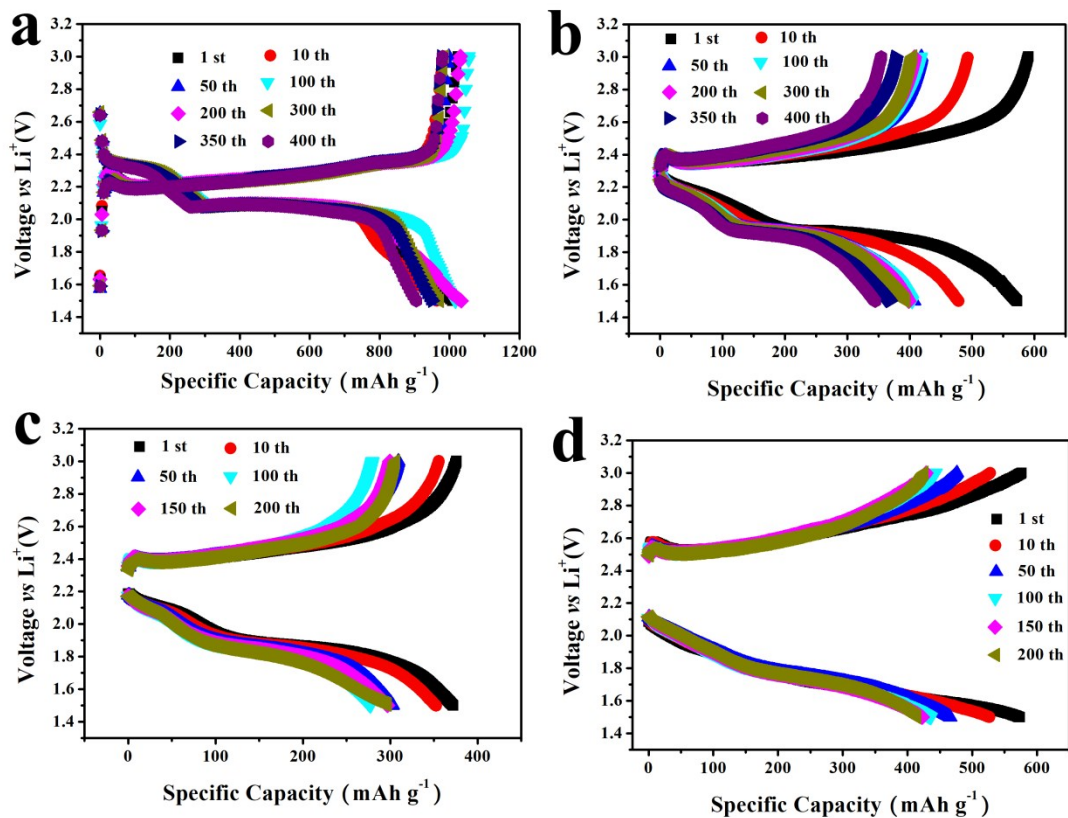


**Figure S23.** Galvanostatic discharge–charge curves recorded at different cycles for 3/S 72%; (a) areal sulfur loading contents of 2.7 mg-sulfur cm<sup>-2</sup> at 1 C; (b) areal sulfur loading contents of 4.2 mg-sulfur cm<sup>-2</sup> at 3 C; (c) areal sulfur loading contents of 4.2 mg-sulfur cm<sup>-2</sup> at 5 C; (d) areal sulfur loading contents of 5.8 mg-sulfur cm<sup>-2</sup> at 1 C.

**Table S1.** The atomic percentages of C, N, O, S and Ni evaluated by XPS.

Composite	C	N	O	S	Ni
1	91.76%	3.33%	4.63%	0.27%	/
2	91.95%	3.99%	3.61%	0.28%	0.17%
3	89.45%	4.99%	2.80%	2.54%	0.22%
4	91.06%	3.63%	3.73%	1.06%	0.52%

**Table S2.** The atomic percentages of different nitrogen species in composites 2, 3 and 4.

Composite	pyridinic-N	pyrrolic-N	graphitic -N
1	1.10%	0.64%	1.59%
2	1.63%	0.87%	1.49%
3	2.12%	0.21%	2.66%
4	1.54%	0.54%	1.55%

**Table S3.** Raman spectra of composites 1-4 and GO.

Composite	I <sub>D</sub> /I <sub>G</sub>
1	1.24
2	1.17
3	1.15
4	1.11
GO	0.95

**Table S4.** Specific surface area and pore volume of composites **1, 2, 3** and **4** evaluated by the Brunauer-Emmett-Teller (BET) and the Barrett–Joyner–Halenda (BJH) method.

<b>Composite</b>	<b>SSA (m<sup>2</sup>/g)</b>	<b>Pore Volume (cm<sup>3</sup>/g)</b>
<b>1</b>	184	0.32
<b>2</b>	477	1.54
<b>3</b>	618	1.73
<b>4</b>	510	1.61

**Table S5.** Specific surface area and pore volume of composites **3'** and **3''** evaluated by the Brunauer-Emmett-Teller (BET) and the Barrett–Joyner–Halenda (BJH) method.

<b>Composite</b>	<b>SSA (m<sup>2</sup>/g)</b>	<b>Pore Volume (cm<sup>3</sup>/g)</b>
<b>3'</b>	599	1.59
<b>3''</b>	610	1.66

**Table S6.** Specific surface area and pore volume of composites **3** and **3/S 72%** evaluated by the Brunauer-Emmett-Teller (BET) and the Barrett–Joyner–Halenda (BJH) method.

<b>Composite</b>	<b>SSA (m<sup>2</sup>/g)</b>	<b>Pore Volume (cm<sup>3</sup>/g)</b>
<b>3</b>	618	1.73
<b>3/S 72%</b>	12	0.11

**Table S7.** The rate performance (mAh g<sup>-1</sup>) of 1/S 72%, 2/S 72%, 3/S 72% and 4/S 72%/Li cells.

Composite	0.2 C	0.5 C	1 C	2 C	3 C	5 C	0.2 C
1/S 72%	945.1	723.7	599.3	516.7	471.6	397.8	673.2
2/S 72%	1078.1	911.3	813.6	742.7	697.7	616.8	900.6
3/S 72%	1534.8	1336.4	1215.5	1074.5	981.1	826.2	1385.7
4/S 72%	1248.4	1004	897.8	799	739.7	672.2	1053.8

**Table S8.** A comparison of cycling performance between this work and some other Li-S cells with long cycle stability reported in literatures.

Cathode materials	Sloading area density (mg cm <sup>-2</sup> )	Cycling performance			Capacity decay rate per cycle (%)	Refs.
		C	cycles	mAh g <sup>-1</sup>		
TiN-S	1.0	0.5	500	988 - 644	0.19	S3
TiS <sub>2</sub> -60S	1.0	1	1000	1021 - 613	0.04	S4
3Mo <sub>2</sub> C/7S	1.0	0.2	300	1200 - 800	0.11	S5
C@SnO <sub>2</sub> /S	1.0	2	1000	745 - 564	0.24	S6
C@TiO <sub>2</sub> @C-S	1.0	2	500	774 - 511	0.068	S7
3/S 72%	1.5	3	1000	959- 732	0.023	<b>This wok</b>

**Table S9.** The rate performance (mAh g<sup>-1</sup>) of 3/S 72%, 3'/S 72% and 3''/S 72%/Li cells.

Composite	0.2 C	0.5 C	1 C	2 C	3 C	5 C	0.2 C
3/S 72%	1534.8	1336.4	1215.5	1074.5	981.1	826.2	1385.7
3'/S 72%	1222.6	1017.3	934.5	864.8	794.9	642.7	1044.8
3''/S 72%	1345.4	1099.5	1027.2	934.3	860.6	732.5	1102.7

**Table S10.** The rate performance (mAh g<sup>-1</sup>) of 3/S 61% and 3/S 81%/Li cells.

Composite	0.2 C	0.5 C	1 C	2 C	3 C	5 C	0.2 C
3/S 61%	1664.5	1381.9	1254.6	1108.2	1013.7	863.9	1453.4
3/S 81%	1346.8	1050.7	978.1	880.6	822.2	762.9	1106.6

**Table S11.** The rate capability (mAh g<sup>-1</sup>) of the cells with as-prepared 3/S cathodes different areal sulfur loading contents of **A** 2.7, **B** 4.2 and **C** 5.8 mg-sulfur cm<sup>-2</sup>

Composite	0.05 C	0.2 C	0.5 C	1 C	2 C	3 C	5 C	0.05 C
<b>A</b>	1333.9	1123.6	1000.9	925.6	840.3	756.3	648.4	1027.8
<b>B</b>	1233.1	1054.6	929.1	790.6	701.3	493.2	380.6	916.1
<b>C</b>	1158.2	1009.7	784.3	574.8	439.8	307.8	149.9	807.2

**Table S12.** A comparison of cycling performance between this work and some other Li-S cells with loading high sulfur area density reported in literatures.

Cathode materials	Sloading area density (mg cm <sup>-2</sup> )	Cycling performance			Capacity decay rate per cycle (%)	Refs.
		C	cycles	mAh g <sup>-1</sup>		
G-VS <sub>2</sub> /S	5.0	0.2	50	1015 - 800	0.42	S8
MC-NS/S	4.5	1	200	586 - 382	0.17	S9
G-NDHCS-S	3.9	0.5	200	839 - 520	0.19	S10
N,S-codoped graphene	4.6	0.5	200	925 - 670	0.16	S11
S@Co-NCNT/NP	3.2	0.5	200	908 - 657	0.15	S12
3/S 72%	5.8	1	200	572- 414	0.14	<b>This wok</b>

## References

- S1. S. L. Yang, H. B. Yao, M. R. Gao, S. H. Yu, *Cryst. Eng. Comm.*, 2009, **11**, 1383-1390.
- S2. D. Y. Go, J. Park, P. J. Noh, G. B. Cho, H. S. Ryu, T. H. Nam, H. J. Ahn, K. W. Kim, *Mater. Res. Bull.*, 2014, **58**, 190-194.
- S3. Z. Cui, C. Zu, W. Zhou, A. Manthiram, J. B. Goodenough, *Adv. Mater.*, 2016 **28**, 6926-6931.
- S4. X. C. Liu, Y. Yang, J. J. Wu, M. Liu, S. P. Zhou, B. D. A. Levin, X. D. Zhou, H. J. Cong, D. A. Muller, P. M. Ajayan, H. D. Abruña, F. S. Ke, *ACS Energy Lett.*, 2018, **3**, 1325-1330.
- S5. X. Q. Zeng, X. H. Gao, G. R. Li, M. H. Sun, Z. Lin, M. Ling, J. C. Zheng, C. D. Liang, *J. Mater. Chem. A*, 2018, **6**, 17142-17147.
- S6. M. X. Wang, L. S. Fan, X. Wu, D. Tian, J. H. Cheng, Y. Qiu, H. X. Wu, B. Guan, N. Q. Zhang, K. N. Sun, Y. Wang, *J. Mater. Chem. A*, 2018, **5**, 19613-19618.
- S7. M. M. Fang, Z. M. Chen, Y. Liu, J. P. Quan, C. Yang, L. C. Zhu, Q. B. Xu, Q. Xu, *J. Mater. Chem. A*, 2018, **6**, 1630-1638.
- S8. X. Y. Zhu, W. Zhao, Y. Z. Song, Q. C. Li, F. Ding, J. Y. Sun, L. Zhang, Z. F. Liu, *Adv. Energy Mater.*, 2018, **8**, 1800201-1800210.

- S9. J. B. Li, C. Y. Chen, Y. W. Chen, Z. H. Li, W. F. Xie, X. Zhang, M. F. Shao, M. Wei, *Adv. Energy Mater.*, 2019, 1901935-1901945.
- S10. G. M. Zhou, Y. B. Zhao, A. Manthiram, *Adv. Energy Mater.*, 2015, **5**, 1402263-1402273.
- S11. G. M. Zhou, E. Paek, G. S. Hwang, A. Manthiram, *Nat. Commun.*, 2015, **6**, 7760-7771.
- S12. T. Chen, B. R. Cheng, G. Y. Zhu, R. P. Chen, Y. Hu, L. B. Ma, H. L. Lv, Y. R. Wang, J. Liang, Z. X. Tie, Z. Jin, J. Liu, *Nano Lett.*, 2017, **17**, 437-444.